Experimental Study of O_2 Diffusion Coefficient Measurement at a Planar Gas–Liquid Interface by Planar Laser-Induced Fluorescence with Inhibition

Mélanie Jimenez, Nicolas Dietrich, Arnaud Cockx, and Gilles Hébrard
Université de Toulouse; INSA, UPS, INP; LISBP, Toulouse, France; INRA, UMR792, Ingénierie des Systèmes Biologiques et des Procédés, Toulouse, France; and CNRS, UMR5504, Toulouse, France

DOI 10.1002/aic.13805
Published online April 27, 2012 in Wiley Online Library (wileyonlinelibrary.com).

A new method for determining the molecular diffusivity of oxygen in liquids is described. The technique was applied through a flat air–liquid interface in a Hele-Shaw cell ($5 \times 5 \times 0.2$ cm^3) and was based on planar laser-induced fluorescence (PLIF) with inhibition. A ruthenium complex ($C_{72}H_{48}N_8O_6Ru$) was used as the fluorescent dye sensitive to oxygen. A mathematical analysis was developed to determine the molecular diffusivity of oxygen simply by localizing the gas diffusion front. The specificity of this mathematical analysis is that it does not require the properties of the fluids (such as the saturation concentration) to be considered, which is especially relevant for complex media that are sometimes difficult to characterize properly. This technique was applied to three different fluids (viscosities ranging from 1 to 2.4 mPa·s) corresponding to binary diffusion coefficients ranging from 9.5×10^{-10} to 2×10^{-9} m^2/s. Experimental data were found with an uncertainty of about 5% and were in good agreement with the literature. Particle image velocimetry and numerical simulations were also carried out to determine the optimal gas flow rate (0.01 L/s) to reach purely diffusive transfer, and the corresponding hydrodynamic profiles of the two phases. © 2012 American Institute of Chemical Engineers *AIChE J,* 59: 325–333, 2013

Keywords: mass transfer, diffusion (mass transfer, heat transfer), PLIF, PIV, gas–liquid interface

Introduction

Gas–liquid mass transfer is of prime interest in several areas,[1] from chemical engineering (bubble column, bioreactors) to environmental issues (waste water treatment, absorption of pollutants in oceans). Because it is a phenomenon related to the efficiency of the processes and to the pollution of natural resources, researches in this area have been many and varied. Nevertheless, some aspects of gas–liquid mass transfer remain unclear and would deserve some additional effort. For instance, a lack of knowledge persists in the molecular diffusivities of gases in liquids and, thus, in the mass-transfer behavior in the vicinity of the gas–liquid interface.

Research in this domain has been intensive, and several techniques have been developed to measure experimental diffusion coefficients of gases in liquids: the diaphragm cell method,[2,3] the capillary cell method,[4,5] the polarographic diffusion cell method,[6] and other techniques based on the use of microprobes,[7,8] the laminar jet method,[9–11] constant/decrease bubble size methods,[12,13] to mention just a few. Optical techniques, such as interferometry, have also been largely developed to characterize diffusive process.[14] Due to their several well-known advantages (fast response, high-resolution, noninvasive nature, reliability of the results, etc.), these techniques seem to be the most suitable ones for studying diffusive mechanisms. However, it has to be noted that they concern gas–gas or liquid–liquid systems in most cases[15,16] and rarely include the measurement of diffusion coefficients of gases in liquid media.[17] As a consequence of the number of techniques available, a multitude of diffusivity measurements exists for a known gas–liquid system and their determination is thus still commonly restricted to the use of empirical correlations (e.g., Refs. 18 and 19) which are valid only under certain conditions (dilute solutions for instance).

Some authors have pointed out the importance and the difficulty of establishing accurate experiments for determining gas diffusion coefficients in liquids.[7–9,20] On the whole, diffusive transfer observations are time-consuming and sensitive to any convective disruption, which complicates the experimental set-up. Moreover, in turbulent media for instance, the thickness of the mass boundary layer can vary from 10 to 100 μm for slightly soluble gases.[20,21] High-resolution systems are thus required for quantitative explorations in the vicinity of the interface and optical systems, such as holographic interferometry, are widely used.[22,23]

The planar laser-induced fluorescence (hereafter, noted PLIF) is another optical system widely used for studying gas transfer in liquids. PLIF[24] is based on the use of a fluorescent dye in the liquid medium, characterized by its sensitivity to specific parameters (gas concentrations, pH changes, etc.). Thanks to this sensitivity, gas absorption can be visualized and concentration profiles can be derived with high spatial and temporal resolutions. PLIF is thus a promising

Correspondence concerning this article should be addressed to M. Jimenez at mjimenez@insa-toulouse.fr, and G. Hébrard at hebrard@insa-toulouse.fr

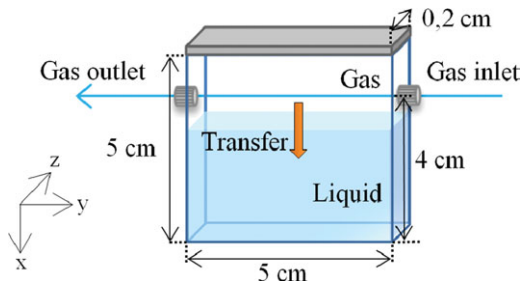

Figure 1. Hele-Shaw cell.

[Color figure can be viewed in the online issue, which is available at wileyonlinelibrary.com.]

technique to shed light on gas–liquid transfer and many PLIF-based studies have been carried out. Wolff et al.[25] introduced PLIF with inhibition to visualize O_2 concentration near a gas–liquid interface. Many researchers, Herlina and Jirka,[21] Wolff and Hanratty,[26] Variano and Cowen,[27] Falkenroth et al.,[28] Asher and Litchendorf,[29] Francois et al.,[30] and among others, have continued to work on the same subject by studying the absorption of O_2 through flat, wavy, or bubble interfaces. Similar experiments have been conducted with other gases such as CO_2[31,32] and HCl.[33] However, despite the various experiments carried out with PLIF on gas–liquid mass transfer, quantitative measurements have focused only on the determination of gas concentration profiles, liquid-side mass-transfer coefficients or mass boundary layer thickness and have mainly concerned turbulent media. To the best of our knowledge, no diffusion coefficient measurements of gases in liquids, which require well-controlled and specific hydrodynamics, have been made using this technique.

The contribution of the work reported here is thus to set-up a new and promising experiment, first to accurately visualize the pure diffusive process of oxygen through a planar air–liquid interface by PLIF with inhibition in a Hele-Shaw cell ($5 \times 5 \times 0.2$ cm^3), then to measure oxygen concentration profile in the liquid phase near the interface, and finally, to determine the diffusion coefficient of oxygen in the studied liquid using a simplified mathematical solution. Experimental results are then compared with values from the literature. The particularity of this article is also that it combines the PLIF technique with particle image velocimetry (PIV) experiments and COMSOL simulations, first, to determine the optimal gas flow rate allowing the diffusive process to take place and then to quantify the hydrodynamic fields in the two phases. This article allows thus two fundamental aspects of gas–liquid transfer to be associated: diffusivity and hydrodynamic behavior.

Determination of mass-transfer equations in a Hele-Shaw cell

Experiments based on a flat air–liquid interface were carried out in a Hele-Shaw cell.[34] This cell's thickness (0.2 cm) is small compared with its height (5 cm) and width (5 cm), as depicted in Figure 1.

With such a configuration, it can be assumed that the problem is two-dimensional (2-D) (the contribution along the z-axis can be neglected), and that a concentration gradient only appears along the x-axis. The absence of convection in the x-direction is also assumed (see "Experimental set-up and procedure" section for further details on the experimental set-up and hypothesis validation).

Under these assumptions, mass-transfer equations in the Hele-Shaw cell can be derived from Fick's law of diffusion[35] as follows

$$\frac{\partial C}{\partial t} = D\frac{\partial^2 C}{\partial x^2} \tag{1}$$

with C the gas concentration in the liquid phase (mg/L), D the molecular diffusivity of the gas in the liquid (m^2/s), t the time (s), and x the distance to the gas–liquid interface (m).

The duration of the experiments being relatively short ($\sim$30 min) compared with the duration of the diffusive process of gas in liquid ($t \sim L^2/D = 833$ min for $L = 1$ cm), the following analytical solution in a semi-infinite medium is assumed[36]

$$\frac{C - C_0}{C_S - C_0} = 1 - \mathrm{erf}\left(\frac{x}{2\sqrt{Dt}}\right) \tag{2}$$

where C_0 and C_s are the concentration in the bulk and at saturation, respectively (mg/L), and erf(·) is the error function defined as in Eq. 3.[37]

$$\mathrm{erf}(u) = \frac{2}{\sqrt{\pi}}\int_0^u \exp(-u^2)\cdot du \tag{3}$$

By setting up an experiment to measure $C(x,t)$ and assuming that C_0 and C_s are known, it is thus possible to determine D using Eq. 2.

However, the knowledge of the saturation concentration C_s is not as simple as wanted, especially in complex media.[6,38,39] This article thus proposes to determine the solution of Eq. 2 in such a way that C_s remains unknown.

Based on Eq. 2, the closed-form expression of $\partial^2 C/\partial x^2$ is given by Eq. 4.

$$\frac{\partial^2 C}{\partial x^2} = \frac{x}{\sqrt{\pi Dt}\cdot 2Dt}\cdot \exp\left(\frac{-x^2}{4Dt}\right)(C_s - C_0) \tag{4}$$

Now, let us introduce the probability density function of a gamma distribution as Eq. 5[40]

$$f(X,k,\theta) = \frac{X^{k-1}\exp(-X/\theta)}{\Gamma(k)\cdot\theta^k} \tag{5}$$

Assuming that D is constant and with $X = x^2$ and $\theta = 4\,Dt$, it can be deduced that Eq. 6

$$\frac{\partial^2 C}{\partial x^2} \propto \frac{X^{1/2}}{\theta^{3/2}}\exp\left(\frac{-X}{\theta}\right) \tag{6}$$

And, thus, that $k = 3/2$ according to Eq. 5.

The relevance of the gamma distribution comes from the fact that its mode, i.e., the value of X maximizing f (X,k,θ) is defined by Eq. 7[40]

$$X_{\max} = (k-1)\cdot\theta, \quad k \geq 1 \tag{7}$$

In this study, the point where $\partial^2 C/\partial x^2$ is maximized at a given time represents the location of the maximum curvature of $C(x,t)$.

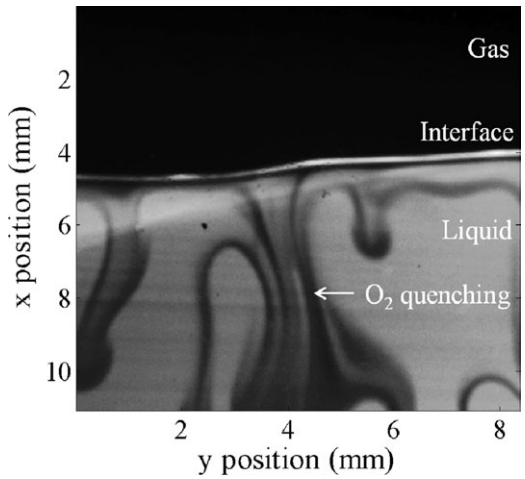

Figure 2. Fluorescence quenching by oxygen in the liquid phase.

The diffusion front is thus characterized by Eq. 8.

$$X_{\max} = x^2_{\text{front}} = \left(\frac{3}{2} - 1\right) \cdot 4Dt = 2Dt \tag{8}$$

However, the time, t, since the beginning of the diffusive process could be quite difficult to determine accurately, it is preferable to study the variation between two subsequent instants.

$$x^2_{\text{front }1} - x^2_{\text{front }2} = 2D(t_1 - t_2) \tag{9}$$

with x_{front} the distance between the gas–liquid interface and the x-position maximizing $\partial^2 C/\partial x^2$.

It is noteworthy that formulation (8) is similar to the Einstein and Smoluchowski equations of Brownian motion[41,42] based on the kinetic molecular theory of gases.[43] However, in our case, the determination of Eq. 8 is directly based on the mathematical resolution of Fick's law and this equation is only valid at a specific and remarkable point, the point of maximum curvature $\partial^2 C/\partial x^2$ for a given time.

The relevance of this formulation has been mathematically proved and experimentally tested as shown in "Results" section.

Thus, according to Eqs. 8 and 9, the method proposed here sets up an experimental technique able to accurately locate the diffusion front, thus the point x maximizing $\partial^2 C/\partial x^2$ and to determine the value of the diffusion coefficient D. Note that no additional properties of the gas or liquid media are required to estimate the molecular diffusion coefficient.

Based on Eq. 9, the uncertainty on the molecular diffusion coefficient determined is given by Eq. 10.

$$\Delta D = \frac{x^2_{\text{front }1} - x^2_{\text{front }2}}{(t_1 - t_2)} \Delta x \tag{10}$$

where ΔD and Δx are the uncertainty on the molecular diffusivity and on the x position, respectively. From Eq. 10, it is straightforward to show that the larger the time scale and the smaller the x uncertainty, the smaller the uncertainty on D. The technique proposed here for visualizing and locating the diffusion of O_2 in liquid is PLIF with inhibition.

Principle of PLIF with inhibition

As details of this subject are available in the literature,[24,44] only the basic principle of the technique is summarized in this section. PLIF, in a gas–liquid complex, is based on the use of a fluorescent dye that is incorporated in the liquid phase. This fluorescent dye is excited by a laser beam and re-emits light (fluorescence phenomenon) to return to its ground state. The light emitted by fluorescence is then recorded by a camera system. The fluorescent dye is chosen for its sensitivity to some parameters such as gas concentration, pH changes, etc. In PLIF with inhibition, the fluorescent dye used is sensitive to the presence of oxygen in the liquid medium. Oxygen molecules inhibit the fluorescence process by colliding with molecules of the fluorescent dye. Due to this collision between molecules,[45,46] oxygen will receive the excess energy of the dye which will return to a ground state by a nonradiative process. O_2 is called a "quencher" of fluorescence. In other words, when no oxygen is present in the liquid, the fluorescence is maximal, leading to a high-light intensity recorded by the camera system. Conversely, when oxygen transfers in the liquid, the fluorescence is inhibited and, thus, darker areas appear (Figure 2).

Thanks to the inhibition of fluorescence, the concentration of O_2 can be determined from the intensity level recorded by the camera. The conversion into oxygen concentration is based on the Stern-Volmer[47] equation

$$\frac{I_Q}{I_0} = \frac{1}{1 + K_{SV}[Q]} \tag{11}$$

where K_{SV} is the Stern-Volmer constant (L/mg), $[Q]$ the quencher concentration (mg/L), and I_Q and I_0 the fluorescence intensities in the presence and the absence of quencher, respectively. The intensity level recorded by the camera, characterized by gray levels, is inversely proportional to the concentration of O_2 in the liquid phase. The calibration curve can be determined by registering the fluorescence level of a solution with a known oxygen concentration, ranging from about 0 mg/L to the saturation concentration. These oxygen concentrations were measured by a specific probe (Mettler Toledo, Nänikon, Switzerland, ±1%). Experimental points always fitted the Stern-Volmer equation with a square correlation coefficient higher than 99% (Figure 3, $K_{SV} = 0.2$ L/mg).

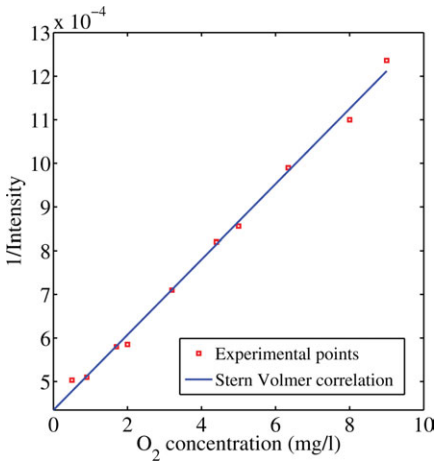

Figure 3. Calibration curve according to the Stern-Volmer equation.

[Color figure can be viewed in the online issue, which is available at wileyonlinelibrary.com.]

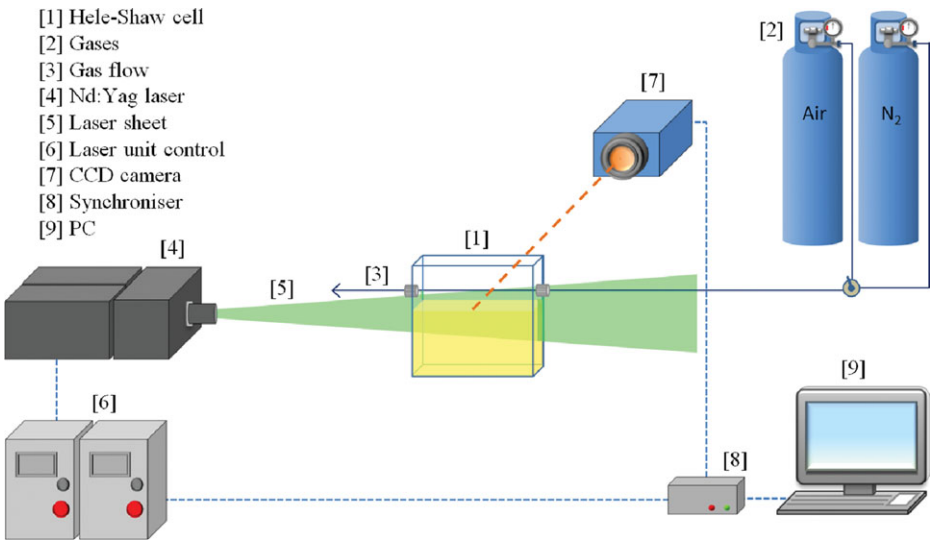

Figure 4. Experimental set-up for PLIF experiments.

[Color figure can be viewed in the online issue, which is available at wileyonlinelibrary.com.]

Experimental set-up and procedure

Experimental Set-Up. The experimental set-up is presented in Figure 4. Each component is explained in detail in the following sections.

As explained in "Determination of mass-transfer equations in a Hele-Shaw cell" section, a Hele-Shaw [1] cell was used to reduce the problem to two dimensions. The Hele-Shaw cell was 5 cm high, 5 cm wide, and 0.2 cm thick (Figure 1). The cell sides were transparent and made of polymethyl methacrylate (PMMA) with two gas orifices placed 1 cm below the top of the cell to allow the gas to flow [3]. An air flow [2,3] of about 0.01 L/s passed tangentially to the liquid interface without disrupting it. The control of the air flow was of prime importance to avoid disruption of the diffusion process by convection (see "Precautions" section).

In accordance with Francois et al.[30] and Dani et al.,[48] the liquid medium filling the Hele-Shaw cell consisted of the studied liquid, 25 mg/L of ruthenium complex (Nanomeps, Toulouse, France), $C_{72}H_{48}N_8O_6Ru$, to observe the fluorescence and 20% by mass of ethanol to solubilize the fluorescent dye. The introduction of ethanol indubitably changed the properties of the liquid phase; however, this does not fundamentally distort the principle presented in this article. The ruthenium complex was chosen for its excellent sensitivity to the presence of oxygen and, thus, its ability to improve the visualization of the O_2 diffusion. Experiments were performed for three different liquid media, whose properties are described in Table 1. Viscosity and density were measured with a Haake VT550 Viscotester (Thermo scientific, Thermo Fisher Scientific, Villebon, France) and with a pycnometer (Brand Duran, Wertheim, Germany, $V = 25$ cm^3), respectively.

The laser sheet [5] was produced by a Nd: Yag laser [4] (Quantel, MT, $\lambda = 532$ nm, 10 Hz, 2×200 mJ) and controlled by a monitoring system [6]. The laser sheet crossed the Hele-Shaw cell vertically, along the *xy* plane. A charge-coupled-device (CCD) camera [7] (Imager Intense, LaVision, Goettingen, Germany, 12 bits) was placed perpendicularly to the Nd: Yag laser, in front of the *xy* plane, to record the fluorescence level at the gas–liquid interface. A range of 2000 gray levels is available with this optical system. The size of the recorded pictures is 1040×1376 pixels^2 which corresponds to a window of $\sim 9 \times 12$ mm^2. A 105-mm objective (Micro-Nikkor 105 mm f/8, Nikon, Champigny, France) and a 570-nm high-pass filter added to the digital camera allowed the fluorescence of the ruthenium complex to be recorded while blocking the laser light. The Nd: Yag laser and the digital camera were synchronized by a synchronizer [8] (Programmable Trigger Unit, LaVision, Goettingen, Germany). Data were then collected using specific acquisition software (Davis 7.2, LaVision, Goettingen, Germany) [9].

Besides PLIF experiments, PIV was carried out to determine the velocity field in the liquid medium. Reflecting particles were added to the liquid medium and their motion was tracked with specific software. The experimental set-up was similar to the one described for PLIF except for the laser used (Dantec Dynamics, Skovlunde, Denmark, Big Sky-Twins Nd: Yag laser, $\lambda = 532$ nm, 15 Hz, 2×30 mJ). The software used to analyze the results was Flow Manager Version 4.60. The tracer particles used were silver-coated hollow glass spheres, 20 μm in diameter, made by Dantec Dynamics. The size of the interrogation areas was 32×32 pixels^2. The delay between two successive images was 32 ms and an overlap of 50% was set.

Experimental Procedure. The first step of the PLIF experiments consisted in determining the calibration curve to check the linearity of the laser and to obtain the conversion equation between gray level and oxygen concentration.

Table 1. Characteristics of the Liquid Media Studied

Case	Water (% w/w)	Ethanol (% w/w)	Glycerol (% w/w)	ρ (kg/m^3)	μ (Pa·s)
1	80	20	0	970	0.0010
2	60	20	20	1029	0.0017
3	50	20	30	1042	0.0024

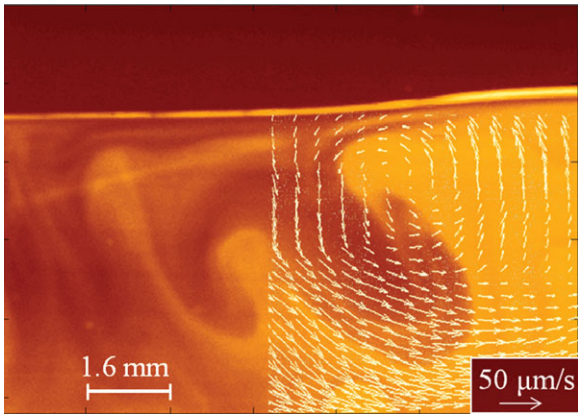

Figure 5. Instabilities at the air–liquid interface due to too high gas flow rates.

[Color figure can be viewed in the online issue, which is available at wileyonlinelibrary.com.]

Then, after the preparation of the liquid medium composed of the studied liquid, ethanol, and the ruthenium complex, the solution was deoxygenated by nitrogen [2] until the oxygen concentration almost reached zero ($\sim$ 0.45 mg/L). Meanwhile, and due to the small thickness of the Hele-Shaw cell, the optical system was precisely adjusted to generate a laser beam flashing between the vertical plates of the Hele-Shaw cell. The deoxygenated solution was then cautiously allowed into the Hele-Shaw cell. The liquid height was set to about 3 cm. A nitrogen flow ran above the interface to insure there was no oxygen intrusion into the liquid medium. After a few minutes, the gas was switched to air to insure an air flow of about 0.01 L/s. The gas switch over corresponded to the time $t = 0$. A laser sheet was generated every minute and five images were recorded simultaneously (10 Hz) each time. It corresponded to a duration of 0.5 s, which is completely negligible in comparison with the duration of the diffusive process. To avoid evaporation issues, the duration of the experiments was limited to about 30 min. The gas–liquid interface was located for each time to check that no evaporation had occurred (see "Image processing" section).

The procedure for PIV experiments was similar to that for PLIF experiments. However, an area sizing the Hele-Shaw cell dimensions was chosen to visualize the whole velocity field in the liquid phase.

Precautions

To insure the accuracy of experiments, some aspects had to be considered with great care. As the Hele-Shaw cell had a small thickness, some capillarity issues were possible. It was of prime importance to limit the apparition of a meniscus because it could lead to a reflection during the laser flash, altering the results.

The insertion of the deoxygenated liquid was a critical step. It had to be carried out in such a way that the interface remained plane and the pollution of the liquid phase by oxygen was limited. A picture was therefore recorded after the insertion of the liquid, while nitrogen flowed above the interface to insure that the interface was effectively flat and that the gray level corresponded to the lowest oxygen concentration determined by the calibration curve.

The gas switch from nitrogen to air had to be done slowly and the interface had to be kept plane without disrupting it. A poorly controlled flow could generate instabilities near the air–liquid interface as shown in Figure 5, where PLIF and PIV experiments are superimposed. Instabilities of this kind can be assimilated to Rayleigh-Taylor finger instabilities.[49,50]

However, when a correct air flow was generated above the interface, no instabilities appeared and the diffusion process could continue. In this case, the velocity field near the air–liquid interface in the liquid phase corresponded to the one depicted in Figure 6.

In this figure, the hypothesis of absence of convection along the x-direction is confirmed at the vicinity of the interface. The weak velocities are due to the configuration of the Hele-Shaw cell, whose walls slow down the liquid motion. It should be noted that, according to PIV experiments, the liquid runs in the side opposed to the gas inlet. In fact, due to the small size of the gas outlet, a loop was also generated in the gas phase. This phenomenon was confirmed by simulations depicted in Figure 7. These simulations were made with the COMSOL Multiphysics 3.5a software and are based on the 2-D space dimension with a laminar flow module and a stationary study type. On this figure, simulations are depicted in the gas phase and PIV results are superimposed to represent the liquid motion.

Experiments were carried out in a temperature-regulated room at 20°C. However, the laser sheet flashing five times a minute on the Hele-Shaw cell could create a temperature gradient, able to generate more convection than described previously. Tests with a thermal camera (FLIR Systems) were conducted to check the temperature homogeneity in the Hele-Shaw cell. The experimental set-up was the same as in the PLIF experiments except that the CCD camera ([7] in Figure 4) was replaced by the thermal camera. The thermal camera only recorded information from the external wall of the Hele-Shaw cell. The temperature of this wall was measured for different numbers of laser flashes, each flash having a duration of a few nanoseconds. It revealed that the thermal gradient in the Hele-Shaw cell could reasonably be neglected as long as experiments required less than 10 successive laser flashes. With five flashes each minute, our experimental set-up was thus assumed to avoid any thermal gradient and induced convection due to the laser sheet.

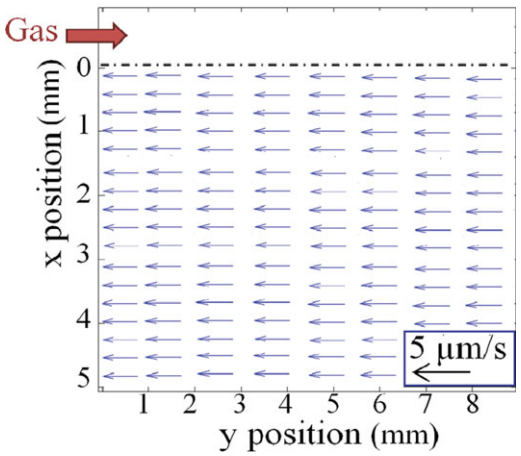

Figure 6. Velocity field in the liquid phase near the interface (Case 1) by PIV.

[Color figure can be viewed in the online issue, which is available at wileyonlinelibrary.com.]

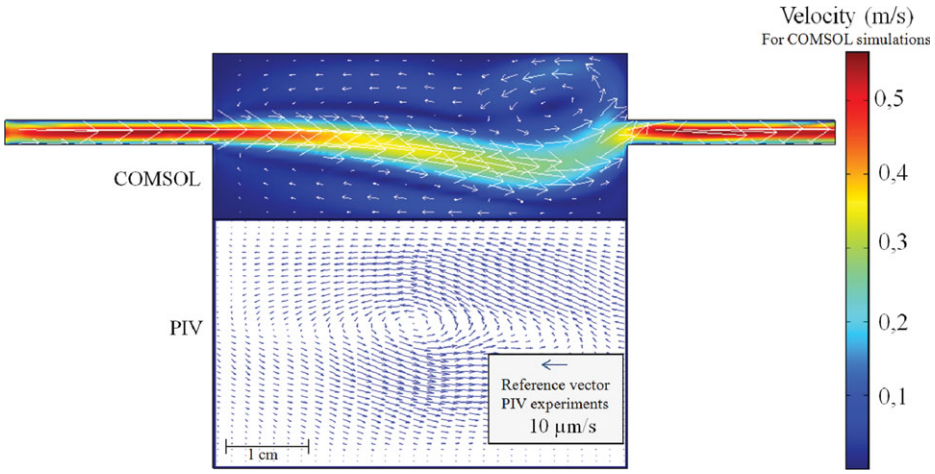

Figure 7. Velocity field (Case 1) in the liquid phase by PIV and in gas phase by COMSOL simulations in the Hele-Shaw cell.

[Color figure can be viewed in the online issue, which is available at wileyonlinelibrary.com.]

Image processing

Pictures registered during the experiments needed some image processing to give accurate quantitative results.

As explained in "Experimental set-up and procedure" section, for each time, five images were recorded at 10 Hz. The first step of the image processing consisted of averaging each pixel over the five pictures to obtain a "mean" picture. This averaging can be considered as a denoising step although it engendered an uncertainty of 0.5 s on the time estimation.

The second step consisted of detecting the gas–liquid interface. Due to reflection at the interface, a peak in the gray values was present in the vicinity of the interface as previously observed.[20,27] As shown in Figure 8, the location of the peak was stable even after several minutes, so there was no evaporation or leakage in the cell. The peak appeared to be quite a Gaussian with a standard deviation corresponding to the interface position uncertainty. This uncertainty was about 13%.

Special precautions have been advised by Walker and Peirson[20] to minimize the area lost by interface reflection. They managed to make oxygen concentration profile measurements within 28 μm of an air–water interface, which is clearly better than the results presented here. However, their experimental set-up required the camera to be inclined (8°). To focus the camera on the liquid interface and to determine the geometric calibration factor (conversion between pixel and millimeters), a ruler was inserted in the Hele-Shaw cell. When the ruler's graduations appeared clear on the recorded image, the focus had been correctly defined. However, an inclined camera also means an inclined ruler to obtain a clear image, which was not feasible in our 2-mm-thick Hele-Shaw cell. A thickness of 7 mm was required to correctly tilt the ruler.

Once the interface was located, the Beer Lambert attenuation due to the absorption of the laser light in the liquid phase had to be considered. This part of the image processing was the same as that described by Walker and Peirson[20] and Falkenroth et al.[28] Because the fluorescent dye concentration was constant in the liquid media, absorption of the laser light depended only on the distance covered by the laser sheet. By modeling the Beer Lambert dispersion, the absorbance coefficient was determined and images were processed to correct this dispersion as shown in Figure 9.

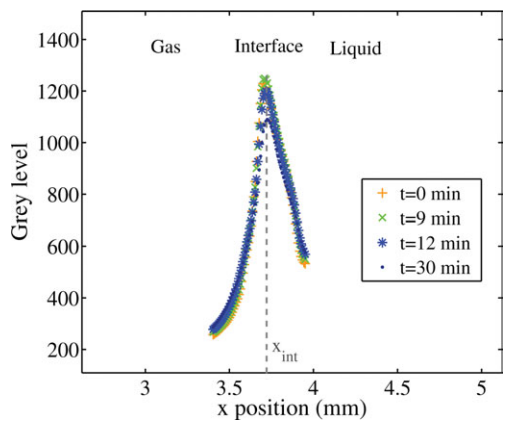

Figure 8. Reflection at the gas–liquid interface.

[Color figure can be viewed in the online issue, which is available at wileyonlinelibrary.com.]

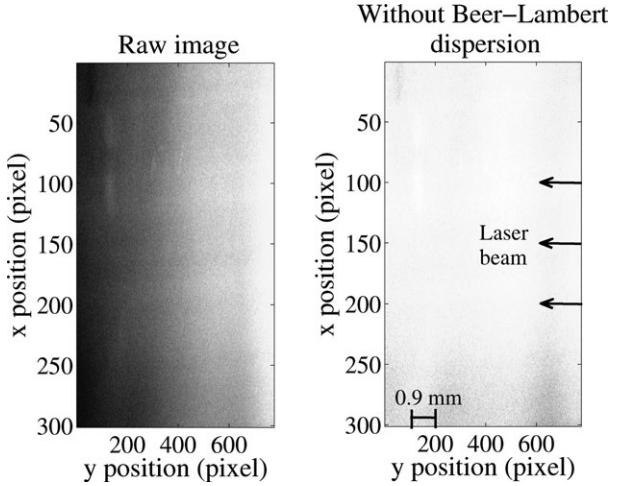

Figure 9. Correction of the Beer Lambert attenuation.

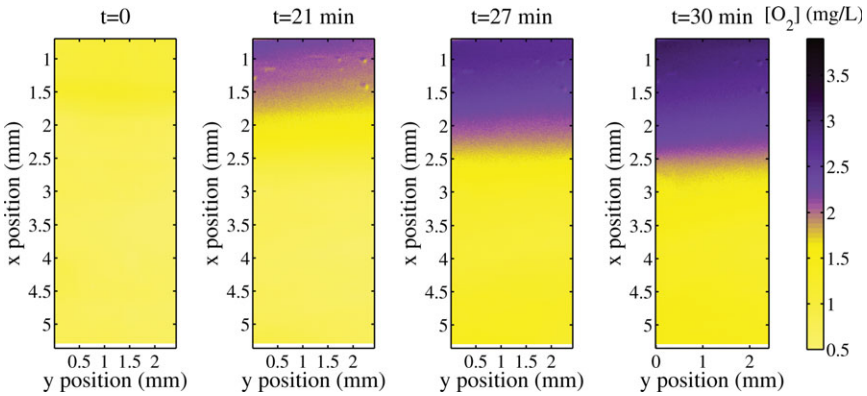

Figure 10. Evolution of oxygen diffusion in the liquid.

[Color figure can be viewed in the online issue, which is available at wileyonlinelibrary.com.]

The last step was the application of a Gaussian filter which averaged a window of 5 × 5 pixels^2 to denoise the raw images.

Results

An example of visualization of the oxygen diffusion process in water (80% w/w) and ethanol (20% w/w) (Case 1) is shown in Figure 10.

At the beginning of the experiments ($t = 0$), the solution had been fully deoxygenated, maximizing the fluorescence and, thus, the intensity recorded by the CCD camera. After some minutes, a plane darker area appeared on the recorded picture, indicating the diffusion of oxygen in the liquid. Times longer than 20 min have been considered in Figure 10 to visualize a sufficient oxygen gradient. Because some micrometers were corrupted in the x-direction due to the interface reflection, the maximum value of oxygen concentration measured near the interface reached almost 4 mg/L in spite of the expected saturation concentration at about 9 mg/L.[6] Similar visualizations were obtained for the two other cases studied (Table 1), but the diffusion process was slower since the viscosity was higher than in Case 1.

Using pictures such as those presented in Figure 10, it is possible to determine the oxygen concentration profile as a function of time, t, and distance to the interface, x. This was achieved by using the Stern-Volmer equation 11 and by averaging each line of the picture to obtain a mean value for each x position.

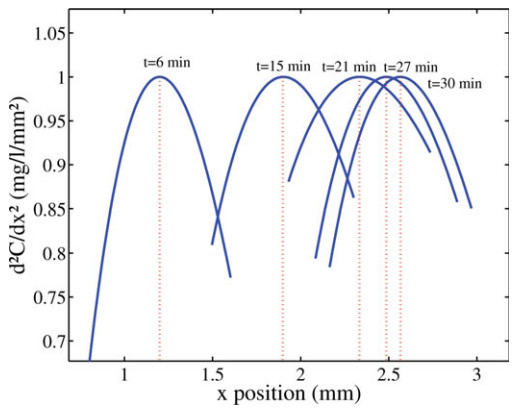

Figure 11. Evolution of the second derivative of *C* with respect to *x*.

[Color figure can be viewed in the online issue, which is available at wileyonlinelibrary.com.]

As explained in "Determination of mass-transfer equations in a Hele-Shaw cell" section, the determination of the oxygen molecular diffusivity requires the location of the diffusion front, and especially the x-position maximizing $\partial^2 C/\partial x^2$ at a given time. To facilitate the determination of this maximum, experimental data were fitted to a sixth-order polynomial, whose second derivative could be easily computed.

Values of $\partial^2 C/\partial x^2$ in the vicinity of the maximal position for study Case 1 are shown in Figure 11.

Note that the location of the maximum, and, thus, of the front, obviously has to increase time after time since the diffusion process goes on. The distance between two successive maxima becomes smaller over time due to Fick's law (Eq. 1). Since oxygen transfers in a fully deoxygenated solution, the exchange potential will become smaller and, thus, the diffusion process slower.

To determine the molecular diffusion coefficient, Eq. 9 was used with all the registered times that minimized the uncertainty on D (Eq. 10). The median value of D was considered as the molecular diffusivity in the liquid studied. Experimental values of D are presented in Table 2 and compared with values from the literature.[18,51]

Good agreement was observed between experimental data and the commonly used correlations related to the determination of molecular diffusivity in aqueous media, confirming the accuracy of the method presented. A comparison among the three liquids studied clearly confirmed the relationship between viscosity and diffusivity. As shown in Figure 12, where slopes are directly proportional to the diffusion coefficients (slope = $2D$), the higher the viscosity, the slower the diffusion process.

These experimental diffusion coefficients present small uncertainties since efforts have already been made to minimize them (Eq. 10). The essential feature of this technique is that the diffusion coefficient measurement is accomplished in a short time (less than 30 min). The accuracy is high (less

Table 2. Experimental Results Compared with Correlations in the Literature

Case	D_{exp} (m^2/s)	$\Delta D/D$	Wilke and Chang[18]	Scheibel[51]
1	1.9×10^{-9}	3%	1.994×10^{-9}	2.02×10^{-9}
2	1.2×10^{-9}	3%	1.3×10^{-9}	1.19×10^{-9}
3	9.47×10^{-10}	5%	9.5×10^{-10}	8.4×10^{-10}

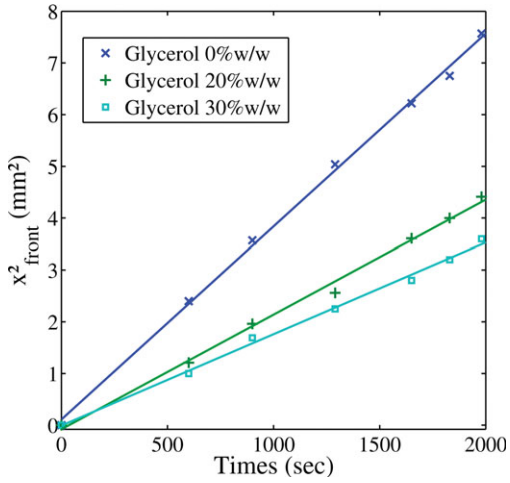

Figure 12. Evolution of x^2_{front} as a function of time for the three cases studied.

[Color figure can be viewed in the online issue, which is available at wileyonlinelibrary.com.]

than 5%), and the amount of fluid necessary to achieve the measurement is small (~3 mL). Another important feature is that only the position and the time of a specific point are necessary for the measurement and no physical properties are required.

It can be noted that if more accurate results are expected for these measurements, specific cares can be done. As shown by Eq. 10, uncertainty on D is directly linked to this of Δx. In the presented experimental set-up, due to the light reflection at the interface, an error is done on the location of the interface (see "Image processing" section). However, to limit this error, it is possible to detect the location in a more precise way by either taking a picture at the initial state before starting the laser flash or by knowing the exact amount of liquid inserted in the cell and, thus, the exact location of the interface. By considering this care, accuracies minor to 1% can be performed. But before considering this approach, it has to be insured that the interface location is actually constant during experiments.

Conclusions

In this article, a new and promising technique was presented to visualize the pure diffusive process of oxygen in an aqueous solution through a flat interface by PLIF with inhibition and to determine the diffusion coefficient of oxygen in liquids. The use of a Hele-Shaw cell allowed the problem to be restricted to a 2-D analysis. Thanks to this simplification, the mathematical determination of the diffusion coefficient was simplified so that it only required the location of the diffusion front vs. time. The proposed approach can also be generalized since other parameters, such as the liquid properties, remain unknown, which is especially relevant in complex media. The PLIF technique with inhibition was relevant since it allowed, first, the pure diffusive process to be visualized and then the oxygen concentration profile to be accurately measured. This technique was validated in three different Newtonian fluids (viscosities ranging from 1 to 2.4 mPa·s) corresponding to binary diffusion coefficients ranging from 9.5×10^{-10} to 2×10^{-9} m^2/s. However, improvements could be made so as to take the interface reflection into consideration. PIV and simulations determined the motion of the two phases and permitted to ensure that only a diffusive process occurred. The results concerning both mass transfer and hydrodynamics were of prime interest since the analytical resolution was based on several hypotheses that needed to be validated. It was shown that, in such a configuration, no convection disrupted the diffusion process when the air flow was correctly chosen. Molecular diffusion coefficients were determined in different liquids to check the relevance of the technique. Good agreement was observed with the literature and uncertainty estimates were small (<5%) with this new technique. The viability of the PLIF technique for measuring diffusion coefficients of oxygen in liquids has been demonstrated in this article. It could thus be generalized to other gases (such as CO_2 if considering pH-sensitive fluorescent dye[32]) and other transparent liquids to become a useful tool for diffusion coefficient measurement and visualization.

Acknowledgments

The financial assistance provided by the French Ministry of Education, Science and Technology and Degremont is gratefully acknowledged. The federation Fermat is also thanked for its help. We are also grateful to Laurent Chatillon and coworkers for their technical support.

Notation

C = gas concentration, mg/L
D = molecular diffusion coefficient, m^2/s
I = fluorescence intensity, gray level
k = parameter of the gamma distribution
K_{SV} = Stern-Volmer constant, L/mg
$[O_2]$ = oxygen concentration, mg/L
[Q] = Quencher concentration, mg/L
t = time, s
V = volume, m^3
x = distance to the interface, m
X = parameter of the gamma distribution
y = tangentially position to x, m

Greek letters

Δx = uncertainty on x position, m
ΔD = uncertainty on D, m^2/s
ρ = density, kg/m^3
μ = viscosity, Pa s
Γ = gamma function
θ = parameter of the gamma distribution
λ = wavelength, nm

Subscripts

0 = gas concentration in the bulk region (C_0), mg/L
= fluorescence intensity in the absence of quencher (I_0), gray level
s = saturation concentration of the gas, mg/L
front = location of the x maximizing the second derivative of C as a function of x

Literature Cited

1. Leahy-Dios A, Firoozabadi A. Unified model for non-ideal multicomponent molecular diffusion coefficients. *AIChE J*. 2007;53:2932–2939.
2. Hung GW, Dinius RH. Diffusivity of oxygen in electrolyte solutions. *J Chem Eng data*. 1972;17:449–451.
3. Tham MJ, Bhatia KK, Gubbins KF. Steady-state method for studying diffusion of gases in liquids. *Chem Eng Sci*. 1967;22:309–311.
4. Malik VK, Hayduk W. A steady state capillary cell method for measuring gas–liquid diffusion coefficients. *Can J Chem Eng*. 1968;46:462–466.
5. Gubbins KE, Bhatia KK, Walker RD. Diffusion of gases in electrolytic solutions. *AIChE J*. 1966;12:548–552.

6. Ho CS, Ju LK, Baddour RF, Wang DIC. Simultaneous measurement of oxygen diffusion coefficients and solubilities in electrolyte solutions with a polarographic oxygen electrode. *Chem Eng Sci*. 1988;43:3093–3107.
7. Hébrard G, Zeng J, Loubiere K. Effect of surfactants on liquid side mass transfer coefficients: a new insight. *Chem Eng J*. 2009;148: 132–138.
8. Jamnongwong M, Loubiere K, Dietrich N, Hébrard G. Experimental study of oxygen diffusion coefficients in clean water containing salt, glucose or surfactant: consequences on the liquid-side mass transfer coefficients. *Chem Eng J*. 2010;165:758–768.
9. Sovova H, Prochazka J. A new method of measurement of diffusivities of gases in liquids. *Chem Eng Sci*. 1976;31:1091–1097.
10. Duda JL, Vrentas JS. Laminar liquid jet diffusion studies. *AIChE J*. 1968;14:286–294.
11. Ferrell RT, Himmelblau DM. Diffusion coefficients of hydrogen and helium in water. *AICHE J*. 1967;13:702–708.
12. Wise DL, Houghton G. The diffusion coefficients of ten slightly soluble gases in water at 10–60°C. *Chem Eng Sci*. 1966;21:999–1010.
13. de Blok WJ, Fortuin JMH. Method for determining diffusion coefficients of slightly soluble gases in liquids. *Chem Eng Sci*. 1981;36: 1687–1694.
14. Ambrosini D, Paoletti D, Rashidnia N. Overview of diffusion measurements by optical techniques. *Opt Lasers Eng*. 2008;46:852–864.
15. He M, Guo Y, Zhong Q, Zhang Y. Determination of binary gas diffusion coefficients using digital holographic interferometry. *J Chem Eng data*. 2010;55:3318–3321.
16. Jamshidi-Ghaleh K, Tavassoly MT, Mansour N. Diffusion coefficient measurements of transparent liquid solutions using Moiré deflectometry. *J Phys D: Appl Phys*. 2004;37:1993–1997.
17. Roetzel W, Blömker D, Czarnetzki W. Messung binärer Diffusionskoeffizienten von Gasen in Wasser mit Hilfe der holographischen Interferometrie. *Chemie Ingenieur Technik*. 1997;69:674–678.
18. Wilke CR, Chang P. Correlation of diffusion coefficients in dilute solutions. *AIChE J*. 1955;1:264–270.
19. Othmer DF, Thakar MS. Correlating diffusion coefficient in liquids. *Ind Eng Chem*. 1953;45:589–593.
20. Walker JW, Peirson WL. Measurement of gas transfer across wind-forced wavy air–water interfaces using laser-induced fluorescence. *Exp Fluids*. 2008;44:249–259.
21. Herlina, Jirka GH. Application of LIF to investigate gas transfer near the air–water interface in a grid-stirred tank. *Exp Fluids*. 2004;37:341–349.
22. Kutepov AM, Pokusaev BG, Kazenin DA, Karlov SP, Vyazmin AV. Interfacial mass transfer in the liquid–gas system: an optical study. *Theor Found Chem Eng*. 2001;35:213–216.
23. Wylock C, Dehaeck S, Cartage T, Colinet P, Haut B. Experimental study of gas–liquid mass transfer coupled with chemical reactions by digital holographic interferometry. *Chem Eng Sci*. 2011;66:3400–3412.
24. Geddes CD. Optical halide sensing using fluorescence quenching: theory, simulations and applications—a review. *Meas Sci Technol*. 2001;12:R53–R88.
25. Wolff LM, Liu ZC, Hanratty TJ. *A fluorescence technique to measure concentration gradients near an interface*. In: Wilhelms SC, Gulliver JS, editors. *Gas Transfer at Water Surfaces*. New York, NY: ASCE Press, 1991:210–218.
26. Wolff LM, Hanratty TJ. Instantaneous concentration profiles of oxygen accompanying absorption in a stratified flow. *Exp Fluids*. 1994;16:385–392.
27. Variano EA, Cowen EA. *Quantitative imaging of CO_2 transfer at an unsheared free surface*. In: Garbe CS, Handler RA, Jähne B, editors. *Transport at the Air-Sea Interface. Environmental Science and Engineering*, Berlin, Germany: Springer, 2007:43–57.
28. Falkenroth A, Degreif K, Jähne B. *Visualisation of oxygen concentration fields in the mass boundary layer by fluorescence quenching*. In: Garbe CS, Handler RA, Jähne B, editors. *Transport at the Air-Sea Interface. Environmental Science and Engineering*. Berlin, Germany: Springer, 2007:59–72.
29. Asher WE, Litchendorf TM. Visualizing near-surface concentration fluctuations using laser-induced fluorescence. *Exp Fluids*. 2009;46: 243–253.
30. Francois J, Dietrich N, Guiraud P, Cockx A. Direct measurement of mass transfer around a single bubble by micro-PLIFI. *Chem Eng Sci*. 2011;66:3328–3338.
31. Takehara K, Etoh GT. *A direct visualization method of CO_2 gas transfer at water surface driven by wind waves*. In: Donelan M, Drennan WM, Saltzman ES, Wanninkhof R, editors. *Gas Transfer at Water Surfaces*. Washington, DC: American Geophysical Union, 2002:89–95.
32. Stöhr M, Schanze J, Khalili A. Visualization of gas–liquid mass transfer and wake structure of rising bubbles using pH-sensitive PLIF. *Exp Fluids*. 2009;47:135–143.
33. Münsterer T, Jähne B. LIF measurements of concentration profiles in the aqueous mass boundary layer. *Exp Fluids*. 1998;25:190–196.
34. Hele-Shaw HS. The flow of water. *Nature*. 1898;58:34–36.
35. Fick A. Ueber diffusion. *Annalen der Physik*. 1855;170:59–86.
36. Crank J. *The Mathematics of Diffusion*. Oxford Science Publications, Oxford, UK, Clarendon Press, 1975.
37. Abramowitz M, Stegun IA. *Handbook of Mathematical Functions with Formulas, Graphs, and Mathematical Tables*. New York: Courier Dover Publications, 1964.
38. Slininger PJ, Petroski RJ, Bothast RJ, Ladisch MR, Okos MR. Measurement of oxygen solubility in fermentation media: a colorimetric method. *Biotechnol Bioeng*. 1989;33:578–583.
39. Schumpe A, Quicker G, Deckwer WD. Gas solubilities in microbial culture media. *Adv Biochem Eng/Biotechnol*. 1982;24:1–38.
40. Upton G, Cook I. *A Dictionary of Statistics*. Oxford, UK: Oxford University Press, 2008.
41. Einstein A. Zur Theorie der Brownschen Bewegung. *Annalen der Physik*. 1906;14:248–258.
42. von Smoluchowski M. Zur kinetischen Theorie der Brownschen Molekularbewegung und der Suspensionen. *Annalen der Physik*. 1906: 326:756–780.
43. Islam MA. Einstein–Smoluchowski diffusion equation: a discussion. *Phys Scr*. 2004;70:120–125.
44. Crimaldi JP. Planar laser induced fluorescence in aqueous flows. *Exp Fluids*. 2008;44:851–863.
45. Lakowicz JR. *Advanced topics in fluorescence quenching*. In: Lakowicz JR, editor. *Principles of Fluorescence Spectroscopy*, 2nd ed. New York, NY: Plenum, 1999; 267–289.
46. Geddes CD, Lakowicz JR. *Topics in Fluorescence Spectroscopy—Part B—Advanced Concepts in Fluorescence Spectroscopy Macromolecular Sensing*, Vol. 10. Springer, 2005.
47. Stern O, Volmer M. On the quenching time of fluorescence. *Physik Z*. 1919;20:183–188.
48. Dani A, Guiraud P, Cockx A. Local measurement of oxygen transfer around a single bubble by planar laser-induced fluorescence. *Chem Eng Sci*. 2007;62:7245–7252.
49. Rayleigh L. Investigation of the character of the equilibrium of an incompressible heavy fluid of variable density. *Proc Lond Math Soc*. 1882;14:170–177.
50. Taylor GI. The instability of liquid surfaces when accelerated in a direction perpendicular to their planes. I. *Proc Roy Soc London Ser A: Math Phys Sci*. 1950;201:192–196.
51. Scheibel EG. Physical chemistry in chemical engineering design. *Ind Eng Chem*. 1954;46:1569–1579.

Manuscript received Nov. 25, 2011, revision received Jan. 26, 2012, and final revision received Mar. 21, 2012.